Journal of Bioscience and Bioengineering
VOL. 127 No. 5, 625–632, 2019

www.elsevier.com/locate/jbiosc

Elucidation of human induced pluripotent stem cell behaviors in colonies based on a kinetic model

Thi Nhu Trang Nguyen,[1] Kei Sasaki,[1,2] and Masahiro Kino-oka[1,*]

Department of Biotechnology, Graduate School of Engineering, Osaka University, 2-1 Yamadaoka, Suita, Osaka 565-0871, Japan[1] *and Global Center for Medical Engineering and Informatics, Osaka University, 2-2 Yamadaoka, Suita, Osaka 565-0871, Japan*[2]

Received 20 August 2018; accepted 18 October 2018
Available online 28 November 2018

Maintaining the homogeneity of a stem cell population is one of the challenges in bioprocessing prior to therapeutic applications of stem cells. Concerning human induced pluripotent stem cell (hiPSC) colonies cultured on feeder cells, cells at the peripheral region of the colony were found to have a higher average movement rate than cells at the central region of the colony. This spatial difference in average movement rate might lead to spatial heterogeneity of cell fate decision in the colony. We have developed a kinetic model to clarify the origin of this phenomenon which was difficult to understand by *in vitro* studies alone. Using a kinetic model based on a cellular automaton, we described fundamental cell behaviors including cell division, contact inhibition, cell migration, cell–cell connections, and cell–substrate connections. With all parameter values estimated from experimental data, the appropriateness of our kinetic model was indicated by good agreement between simulated and experimental data. Using the kinetic model, the average cell movement rate in a colony became homogenous after cell division stopped, implying that cell division was the main cause of the observed spatial heterogeneity. The result also showed a directly proportional relationship between the frequency of cell pushing and cell movement rate in the colony, confirming the role of cell division. Our kinetic model is expected to be useful for studying behaviors of hiPSCs and proposing good strategies to improve hiPSC bioprocessing.

[**Key words:** Kinetic model; Human induced pluripotent stem cells; Heterogeneity; Division; Contact inhibition; Migration; Cell-cell connection; Cell-substrate connection]

For decades, stem cells have been used in regenerative medicine and drug screening due to their capabilities of self-renewal and differentiation into various cell types. However, there are still many challenges in stem cell processing that need to be overcome prior to their routine therapeutic application. One such challenge is that the heterogeneity of propagated stem cell populations makes it difficult to control the quality of the final products. Many efforts have been made to maintain the homogeneity of stem cell populations in culture by developing new cell culture platforms, extracellular components, or maintenance methods (1–3). Understanding the mechanism as well the origin of the heterogeneity in a cell population is the core issue. Some research groups have focused on the heterogeneity of stem cell colonies or aggregation where positional heterogeneity of the cell state was observed (4–6).

For more efficient cell manufacturing processes, there is a need to apply computer analyses instead of only relying on the empirical knowledge of professionals. Computational modeling can be used to manage processes non-invasively, control product quality, elucidate the mechanism of the phenomenon of interest, and predict the outcome. The strengths of computational modeling are that it is high-speed, economical, and able to easily satisfy many conditions that are impossible to be realized in reality. In many cases, computational modeling has been successfully used to predict stem cell fate as well provide insights into the mechanism underlying some processes. To the best of our knowledge, the first model of stem cells was published in 1963 which described the proliferation of hematopoietic stem cells during the growth of spleen colonies (7). In the context of stem cell biology, almost all models focus on cell self-renewal, cell-fate specification, and cellular reprogramming in the case of hiPSCs (8–10). Generally, stem cell models can be divided into two groups: continuum models and cell-based models. Continuum models are usually developed from ordinary or partial differential equations that simulate the average of the whole cell population rather than individual cells. A coarse-scaled continuous model is suitable for understanding the stability and general qualitative features of the cell population. In contrast, cell-based models, including on-lattice models such as cellular automata (CA) and off-lattice models, simulate the multicellular system at the single-cell level, and therefore, are more appropriate for quantitative analysis and describing the heterogeneity of a cell population.

With the goal of developing a module-based simulator, we can describe various cell types by selecting suitable modules among previously developed ones. Our modules described not only cell behaviors but also culture manipulation and the culture environment such as seeding and medium change conditions. Combining all necessary modules, we were able to express processes and phenomena in cell culture and tissue construction, then analyze

* Corresponding author. Tel.: +81 6 6879 7444; fax: +81 6 6879 4246.
E-mail address: kino-oka@bio.eng.osaka-u.ac.jp (M. Kino-oka).
Much of this work forms the basis of the Ph.D. dissertation of Thi Nhu Trang Nguyen.

1389-1723/$ – see front matter
https://doi.org/10.1016/j.jbiosc.2018.10.016

aspects of biology and biophysical chemistry computationally. Previously, our group successfully developed models for culturing keratinocytes, chondrocytes, and skeletal muscle myoblasts (11–13). With a CA approach, we modeled behaviors of a single cell and analyzed conditions at higher levels such as in a culture vessel. By executing numerical simulations, we were able to optimize culture conditions for the effective expansion of those cells. We investigated the influence of inoculum size on the growth of keratinocytes by considering the cell placement and contact inhibition (11). Furthermore, when extended to three-dimensional culture of chondrocytes embedded in the collagen gel by considering oxygen transfer, our model supported the understanding of spatial distribution of cells in a gel as well as the extents of oxygen supply (12). Most recently, by describing the cell migration on culture surface, the adverse effect of non-uniform cell seeding on the growth of skeletal muscle myoblasts was described (13).

Our recent interest is the behavior of hiPSCs in colonies cultured on feeder cell layers. We observed heterogeneity in the cell movement rate of cells within a colony: the average cell movement rate at the peripheral region of the colony was higher than that at the central region of the colony (14). Therefore, we used computational modeling to understand what caused this heterogeneity in the colony which was difficult to clarify by *in vitro* study alone. Compared to our previous studies, here we further develop the model to describe the balance between cell migration, cell-cell connections, and cell-substrate connections that is important in hiPSC behaviors. Our developed model is expected to be useful for studying behaviors of hiPSCs in colonies and gives us good strategy to maintain the homogeneous state of hiPSCs that is crucial in stem cell processing.

MATERIALS AND METHODS

***In silico* colony seeding** We used a two-dimensional CA which consists an array of cubes having a finite number of states and can change their states at each time step according to our developed rules. The simulation was initiated by seeding single or multiple colonies depending on the purpose of the experiment. In this seeding process, the adhesion time and lag time were assumed to be negligible and the attachment ratio was assumed to be one. Other assumptions were indicated in our previous publication (13). The flow of numerical simulation is shown in Fig. S1. After seeding, simulations were run with four cell behaviors followed by the increase of t by a time step Δt of 0.1 h.

***In silico* rules of cell connection** Cells form cell-cell connections with other cells or cell-substrate connections with the substrate through cadherin- and integrin-mediated interactions. In this model, we focused on the energy that a cell utilizes to form cell-cell and cell-substrate connections. Cell-cell and cell-substrate connection energies are defined as E_{cc} and E_{cs}, respectively. When a cell makes a connection with another cell or the substrate cube, the distance between them should be small. In this model, when the distance between the center of a cell or substrate unit cube and that of the target cell cube was not more than $\sqrt{2}l_c$, the unit cube could make a connection with the target cell. When a pair of cells i and j made a connection, the connection energy between them was given by $E_{cc} = \min(E_{cc,i}, E_{cc,j})$. The connection energy between cell c and the substrate is given by $E_{cs} = E_{cs,c}$.

***In silico* rules of cell migration** *In vivo* and *in vitro* cell migration is a complex process involving drastic changes in the cellular cytoskeleton and the continuous breaking and formation of cell interactions. In this model, the migration process was simplified where a cell uses energy to break and form cell-cell and cell-substrate connections immediately and the remaining energy will be used for migration. Cells can migrate in one of eight distinct directions ($N_d = 8$) denoted by the variable dir, which are assigned from north ($dir = 0$) to northwest ($dir = 7$) in a clockwise manner. For each time step, a cell migrates to one of the eight nearest neighbor (NN) cubes on substrates or stays within the current cube. To describe the migration of cell c in the direction dir with the rate of $V_{m,c}$, first the cell migrates to the NN cube located in the direction dir of the current cube, then the variable $t_{m,c}$, a waiting time for the next migration, is updated as $t_{m,c} = l \cdot V_{m,c}^{-1}$, where l is the migration distance given by $l = l_c$ when dir is even or $\sqrt{2}l_c$ when dir is odd. The waiting time $t_{m,c}$ decreases by Δt for each time step. If the waiting time is maintained ($t_{m,c} > 0$), then this cell does not actively migrate, but can be passively exchanged with the NN cells whose waiting times are less than zero.

When the waiting time of cell c becomes less than or equal to zero ($t_{m,c} \le 0$), the direction dir and the rate $V_{m,c}$ of migration are determined by the following rules. First, the direction dir is determined stochastically based on the probability $Pr_{m,dir}$. This probability is basically given by the normalized quantity $p_{m,dir}$ which is proportional to (i) the term relating to the connection energy between the target cell cube and the other cell and/or substrate cubes reduced by the migration ($R_{m,dir}$), (ii) the weight for randomly selecting a space (Ω_{dir}) as described previously (11), and (iii) the possibility of displacement ($H_{m,dir} = 0$ or 1).

We defined a weight for occurrence of migration to the direction dir as follows:

$$R_{m,dir} = 1 - \frac{E_{B,dir}}{E_A} \tag{1}$$

where E_A and $E_{B,dir}$ are the total connection energy formed by the cell of interest before migration and the total reducing connection energy due to migration to the direction dir, respectively. E_A is defined by the following equation:

$$E_A = \sum_{dir=0}^{N_{nn}-1} E_{c,dir} \tag{2}$$

where E_c is either E_{cc} or E_{cs}, N_{nn} is the number of NN cubes ($N_{nn} = 13$ in 2D culture (Fig. S2)).

$E_{B,dir}$ is defined as the equation below and must not exceed the maximum migration energy E_{max}.

$$E_{B,dir} = \sum_{dir=0}^{N_{nn}-1} \Delta E(d; dir) \tag{3}$$

where $\Delta E(d; dir)$ is the reduced amount of connection energy between the target cell and the nearest neighbor cubes when the target cell moves in the direction dir.

The cells cannot migrate to a position where the cell cannot make any connections with other cells or the substrate. In other words, the migration can occur when there is at least one other cell or substrate cube with which the target cell can make a connection in new destination. If this condition is violated, migration does not occur. In this case, we defined the possibility of displacement to be zero: $H_{m,dir} = 0$. Otherwise, $H_{m,dir} = 1$ is given.

In a case when there are no other cells neighboring a target cell, and thus the migration cannot be executed by replacing the positions with a cell in the vicinity, the probability for selecting dir as the direction of migration $p_{m,dir}$ is given by

$$p_{m,dir} = \frac{R_{m,dir}\,\Omega_{dir}\,H_{m,dir}}{\sum_{dir'=0}^{N_d-1}\left(R_{m,dir'}\,\Omega_{dir'}\,H_{m,dir'}\right)} \tag{4}$$

In a case when the denominator becomes zero, we did not calculate the probability because the target cell cannot migrate in any direction.

In general cases, including a case executing the replacement of the positions with a cell in a neighboring target cell, the probability for selecting dir as the direction of migration is given by

$$Pr_{m,dir} = \frac{\left(p_{m,dir}\right)_T\left(p_{m,\widetilde{dir}}\right)_D}{\sum_{dir'=0}^{N_d-1}\left(p_{m,dir'}\right)_T\left(p_{m,\widetilde{dir'}}\right)_D} \tag{5}$$

where $(p_{m,dir})_T$ represents the probability that the target cell selects dir as the direction of migration as if there are no other neighboring cells, and $(p_{m,\widetilde{dir}})_D$ represents the probability that another cell exists at the destination selects the direction opposite to dir (designated as $\widetilde{dir}$). If there is no other cell at the destination, then we substitute 1 for $(p_{m,\widetilde{dir}})_D$. In this case, we have $Pr_{m,dir} = p_{m,dir}$.

When the cell migrates in the direction dir, the total reducing connection energy $E_{B,dir}$ is subtracted from the maximum energy that can be used for the migration (E_{max}). The remaining energy is used for the migration:

$$\frac{1}{2}m_c V_{m,c}^2 = E_{max} - E_B \tag{6}$$

where $V_{m,c}$ and m_c are the cell migration rate and the mass of cell c, respectively, and

$$E_{max} = \frac{1}{2}m_c V_{m,free}^2 \tag{7}$$

is given, where $V_{m,free}$ represents the migration rate when no connection is broken. Using the two equations above, we obtained the following relationship:

$$V_{m,c} = V_{m,free}\sqrt{1 - E_B/E_{max}} = V_{m,free}\sqrt{1 - i\varepsilon_{cc} - j\varepsilon_{cs}} \tag{8}$$

where ε_{cc} ($\varepsilon_{cc} = E_{cc}/E_{max}$) and ε_{cs} ($\varepsilon_{cs} = E_{cs}/E_{max}$) are ratio of energy for cell-cell and cell-substrate connection in maximum energy, and i and j are the number of broken cell-cell and cell-substrate connections, respectively.

***In silico* rules of cell division** After sufficient preparation of genetic material and mass in each cell cycle, a proliferating cell divides into two identical daughter cells that continue to grow to their full size. Here, we describe only the duplication of

one mother cell into two identical daughter cells and ignore the change in cell size. Proliferating cells divide every generation time t_g which is a stochastic variable given randomly from $[0.9\overline{t_g},\ 1.1\overline{t_g}]$ (uniform distribution) at the beginning of each cell cycle. The parameter $\overline{t_g}$ is the mean generation time and is estimated by $\ln(2)/\mu_p$, where μ_p is a specific growth rate of cell culture. Each cell has a waiting time for the next division $t_{d,c}$ which equals t_g at the time of cell birth and is decreased by Δt for each time step. When the waiting time is less than or equal to zero and there is at least one vacant NN cube, this cell can divide and update $t_{d,c}$ as $t_{d,c} = t_{d,c} + t_g$. During cell division, the mother cell puts its daughter cell on one of the vacant NN cubes stochastically as described previously (11). If there is no vacant NN cube, the mother cell first selects one of the vacant cubes closest to it, then one of the NN cells of the selected vacant cube is moved to that cube. The procedure is repeated until the mother cell has a vacant NN cube in which to place the daughter cell.

***In silico* rules of cell quiescence** Due to contact inhibition of cell division, cells cannot divide and become quiescent. We assumed that whenever a cell is surrounded by other cells and there is no vacant space in the distance N_c from the center of it, this cell enters a quiescent state. If the cell is in the quiescent state, the waiting time for the next division does not decrease for each time step. Whenever a vacant space appears at the distance N_c from the center of a quiescent cell, this quiescent cell returns to a non-quiescent proliferative cell state at the next time step.

***In silico* culture of hiPSCs** *In silico* culture was executed in the LabVIEW (National Instruments Corp., Austin, Texas, USA) environment on the commercially available workstation (Precision T7500 workstation, Dell Inc., Round Rock, Texas, USA).

***In vitro* culture of hiPSCs** hiPSCs (clone Tic, JCRB1331) were maintained in 55-cm^2 dishes (Corning Costar, Cambridge, MA, USA) with feeder cells SNL 76/7 (European Collection of Cell Cultures, Salisbury, UK) or mouse embryonic fibroblasts (MEFs) (ReproCELL Inc., Tokyo, Japan) on 0.1% gelatin-coated surfaces at 37°C, 5% CO_2. The medium ReproStem (ReproCELL Inc.) containing 5 ng/mL basic fibroblast growth factor was used. hiPSCs were subcultured every 5 days. More details about *in vitro* culture are mentioned in our previous paper (14).

Analysis of movement rate of hiPSCs in colony We analyzed cell movement rates of individual cells in a colony, which was calculated by the displacement of a cell divided by the duration of the movement time as shown in the following equation:

$$V_c = \frac{\sqrt{(X_t - X_{t-dt})^2 + (Y_t - Y_{t-dt})^2}}{dt} l_c \tag{9}$$

where (X_t, Y_t) and (X_{t-dt}, Y_{t-dt}) are coordinates of a cell at culture time t h and $(t - dt)$ h; l_c is the length of the unit cube.

For *in vitro* cell tracking, cell nuclei were stained with Hoechst 33342 (Thermo Fisher Scientific, Waltham, MA, USA) and live images were captured every 30 min during the culture for 6 h (14). Depending on the purpose of the experiment, t and dt were determined as different values. t and dt were determined to be 54 h and 6 h, respectively, as was used in our previous paper (14) to estimate cell migration-related parameters. The average movement rate against the distance from the center of the colony $\overline{V_R}$ was calculated by taking an average of cell movement rate V_c of all cells at every 100 μm from the center of the colony at $t = 50$ h, 90 h, 128 h, and $dt = 6$ h. Average cell movement rate V_M is the average of cell movement rate V_c of all cells at the central and peripheral regions of the colony, which were determined as the 4 inner- and outermost cell layers of the colony, respectively. It was estimated at $t = 72$ h, 96 h, 120 h, 144 h, and $dt = 24$ h to investigate the relationship between pushing frequency and average cell movement rate.

Analysis of cell movement rate toward the outside of colony, $V_c \cos\theta$ At $t = 48$ h, the central and peripheral regions of the colony were determined as the 4 inner- and outermost cell layers of the colony, respectively. Cells at the central and peripheral regions of the colony were analyzed to determine their movement rate toward the outside of colony, $V_c \cos\theta$, from $t = 48$ h to $t = 54$ h. Angle θ was determined by $180° - \mathrm{O\widehat{A_c}B_c}$ where O is the center of the colony, A_c and B_c are positions of cell c at $t = 48$ h and $t = 54$ h, respectively. A negative $V_c \cos\theta$ indicated an inward movement to the center of colony. Non-negative values indicated outward movement to the outside of colony. Frequencies of cells with different value ranges of $V_c \cos\theta$ in three single *in silico* colonies were analyzed.

Tracking cell movement *in silico* At $t = 24$ h, three cells at the central region and at the edge of colony cultured on MEF feeder cells were tracked every 30 min for 120 h. Tracked cells at the central region and edge of the colony were marked in yellow and red, respectively. Other cells in the colony were marked in blue. The pushed cells that led to the movement of tracked cells were marked in green. Cell tracking was processed by ImageJ software.

Calculation of average frequency of being pushed Average frequency of being pushed is the average of the frequency that one cell at the central or peripheral region of the colony was pushed out due to the division of other cells. The frequency of one cell being pushed P_c (times/h) was calculated by the following equation:

$$P_c = \frac{\text{Times being pushed from}(t - dt) \text{ to } t}{dt} \tag{10}$$

where $t = 72$ h, 96 h, 120 h, 144 h, $dt = 24$ h.

Least-squares method The least-squares method was used to find the best fit value of the contact inhibition-related parameter N_c and migration-related parameters $V_{m,free}$, ε_{cc}, and ε_{cs}.

Statistical analysis Mann−Whitney U test was used to validate simulated results of colony size distribution in the culture vessel against experimental data at 24 h and 120 h after seeding at a significance level of 0.05 (number of colonies: $n > 50$).

RESULTS

Estimation of model parameter values Before executing a simulation to express culture profiles as well as to elucidate cell behaviors in a colony, all parameter values need to be estimated. The length of a side of the unit cube l_c was estimated as the square root of the averaged cell area A_c which equaled 329 μm^2 and 426 μm^2 in cultures of hiPSCs on SNL and MEF feeder cells, respectively, as estimated from independent experiments. Therefore, the unit cube length was estimated to be 18.1 μm and 20.6 μm in culture on SNL and MEF feeder cells, respectively.

Mean generation time was calculated by $\ln(2)$ divided by the specific growth rate of hiPSCs in culture. The mean generation time, $\overline{t_g}$, of hiPSCs in culture on SNL and MEF feeder cells was estimated to be 15.8 h and 21.5 h, respectively.

The following four parameters were estimated by fitting to experimental data using the least-squares method: number of cell layers for occurrence of contact inhibition N_c, free migration rate $V_{m,free}$, ratio of cell-cell connection ε_{cc}, and ratio of cell-substrate connection ε_{cs}. The number of cell layers for the occurrence of contact inhibition N_c was estimated by fitting to the experimental growth profile of 26 colonies of undifferentiated cells shown in Fig. 1. To simulate the growth profile of colonies on a computer, the procedure is described below. A single colony was seeded with radius of 9 and 7 cell layers in culture on SNL and MEF feeder cells, respectively. The seeding radius was determined as the average radius of 26 *in vitro* colonies at 24 h. We changed the value of N_c in the range of [1, 10] (cell layer) and searched for the value that gave the best fit simulated growth curve. The best fit values of N_c were determined to be 7 cell layers (coefficient of determination $R^2 = 0.99$) and 8 cell layers (coefficient of determination $R^2 = 0.99$) in culture on SNL and MEF feeder cells, respectively.

Average cell movement rate at the central and peripheral regions of 10 *in vitro* colonies in culture on SNL and MEF feeder cells at 48−54 h were used for fitting parameter values. For *in silico* culture, we seeded a single colony with a radius of 10 cell layers until the size of colony reached 0.5 mm^2, then the movement rates of cells at the central and peripheral regions were calculated. We changed the value of $V_{m,free}$ in the range of [1.0, 15.0] (μm/h), ε_{cc} and ε_{cs} in the range of [0.05, 0.35] (−), and searched for the combination of their values that gave the movement rate that best fit the experimental data. The combination ($V_{m,free}$, ε_{cc}, ε_{cs}) was determined as (4.0 μm/h, 0.15, 0.05) and (4.0 μm/h, 0.05, 0.15) when cultured on SNL and MEF feeder cells, respectively. Simulated average movement rate of hiPSCs at the central and peripheral region were 2.9 ± 1.9 μm/h and 5.6 ± 3.3 μm/h or 3.6 ± 2.3 μm/h and 5.6 ± 3.3 μm/h when cultured on SNL or MEF feeder cells, respectively (Fig. 2).

Validation of the model With all estimated parameters, we simulated the growth of hiPSCs cultured on SNL and MEF feeder cells for 144 h (Movies S1 and S2). Using different culture data from the data used for fitting N_c in previous results, we estimated the position and size of every single colony in culture vessels at $t = 24$ h and used them as input data for *in silico* culture. Further, we calculated cell density in culture vessels every 24 h and colony size at $t = 120$ h, then simulated and experimental data were compared. Experimental data in Fig. 3 represent the mean cell density from 3 culture vessels. The growth curves obtained by the simulation were very similar to the experimental data with high coefficients of

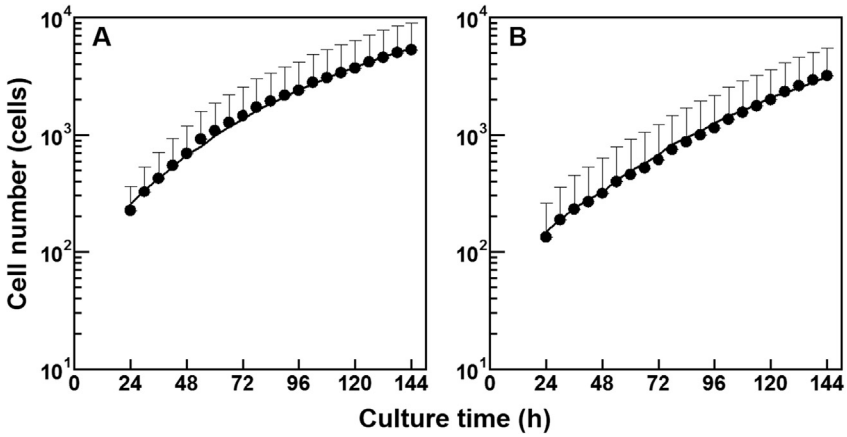

FIG. 1. Estimation of contact inhibition by fitting to time profiles of hiPSC colonies with undifferentiated cells in cultures on SNL (A) and MEF (B) feeder cells. Closed circle: *in vitro* data; Line: best fit *in silico* data.

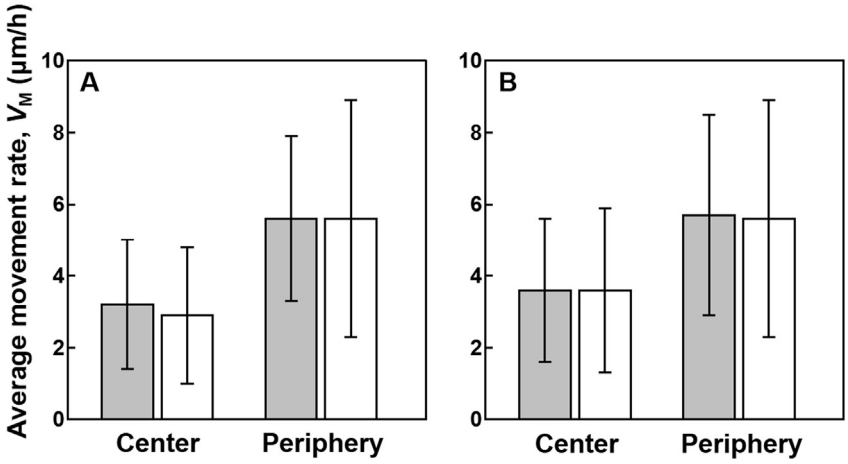

FIG. 2. Estimation of $V_{m.free}$, ε_{cc}, and ε_{cs} by fitting to the average movement rate at the central and peripheral regions of hiPSC colonies cultured on SNL (A) and MEF (B) feeder cells. Shaded bars, experimental results obtained from 10 colonies. Open bars, best fit simulation results obtained by the least-squares method. Standard deviations were calculated from all cells in colonies ($n \geq 300$).

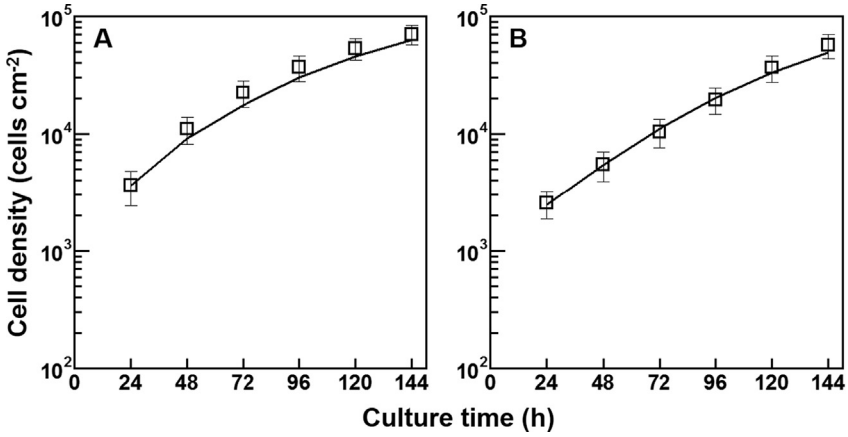

FIG. 3. Time profiles of hiPSCs in culture wells with only undifferentiated cells cultured on SNL (A) and MEF (B) feeder cells. The data represent analytical results obtained from 3 wells. Square, *in vitro* data; line, *in silico* data.

determination R^2 of 0.94 and 0.97 in culture on SNL and MEF feeder cells, respectively. Fig. 4 shows the boxplot for experimental and simulated distributions of colony size in 3 culture vessels. Our results showed good agreement between simulated and experimental distribution of colony size at $t = 24$ h and $t = 120$ h. Mann–Whitney U test indicated no significant difference between *in vitro* and *in silico* distributions of colony size in culture vessels ($P > 0.05$).

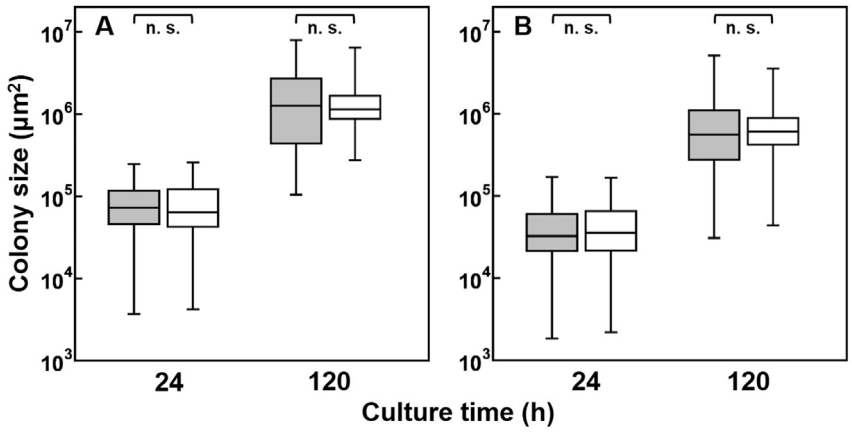

FIG. 4. Distribution of colony sizes obtained under culture on SNL (A) and MEF (B) feeder cells at 24 h and 120 h after seeding. Shaded box, *in vitro* data; open box, *in silico* data. In each box plot, the central point represents the median, the box gives the interval between the 25% and 75% percentiles, and the whisker indicates the range.

Supplementary video related to this article can be found at https://doi.org/10.1016/j.jbiosc.2018.10.016.

To validate our model regarding cell migration behavior in colonies, we examined the cell movement rate toward the outside of colony at the central and the peripheral regions. The results showed similar trends of cell movement direction between *in silico* and *in vitro* colonies. In colonies cultured on SNL feeder cells, cells moving toward the outside of the colony made up 67% of the central region and 87% at the peripheral region of *in silico* colonies (Fig. S3A, E). Those frequencies were 71% at the central region and 96% at the peripheral region for *in vitro* colonies (Fig. S3B, F). A similar trend occurred in colonies cultured on MEF feeder cells where there were more cells moving toward the outside of colony than that at the central region of colony (*in silico*: 65% at the central region and 86% at the peripheral region; *in vitro*: 66% at the central region and 98% at the peripheral region) (Fig. S3C, D, G, H).

Elucidation of cell movement behavior in colonies To understand more about the heterogeneity of cell movement rates in a colony, the spatial and temporal dependence of cell movement rate were analyzed. We simulated a single colony and calculated the average movement rate $\overline{V_R}$ of all cells at every 100 μm from the center of the colony at t = 50 h, 90 h, and 128 h during colony expansion so that the colony radiuses reached 300 μm, 500 μm, and 700 μm, respectively (Fig. 5). Parameter values of hiPSCs cultured on MEF feeder cells were used. We observed two distinct parts of cells including quiescent cells at the central region of the colony and proliferating cells at the peripheral region of the colony (Fig. 5A–C). At t = 50 h, almost all cells in the colony were proliferating (Fig. 5A) and the average cell movement rate increased when the distance from the center of the colony R increased (Fig. 5D). At t = 90 h and 128 h, a contact inhibition region appeared from R = 0 μm to R = 300 μm in Fig. 5E and from R = 0 μm to R = 500 μm in Fig. 5F. The analysis showed that the average movement rates of cells in colonies were homogeneous in the contact inhibition region but heterogeneous in the proliferating ring at the edge of the colony. In addition, the average cell movement rate in the contact inhibition region did not change much during colony expansion. On the contrary, in proliferating rings at the periphery of the colony, the average cell movement rate increased to the highest value at the outermost edge of the colony and this highest average cell movement rate was approximated at different time points. Fig. 5 shows the temporal independence and spatial dependence of the average cell movement rate in a colony of hiPSCs.

The difference in average cell movement rate between the contact inhibition region and proliferating region in Fig. 5 implied that cell division might be the factor leading to the heterogeneity of cell movement rate in colonies. Therefore, we stopped cell division by setting the value of $\overline{t_g}$ to infinity or stopped cell migration by setting the value of $V_{m,free}$ to zero to clarify the effect of cell division on cell movement rate. The results showed different scenarios of cell movement in colonies between three simulated conditions (Movies S3–S5). Results presented in Fig. 6A–C are a heat map of the cell movement rate V_c at t = 128 h when the colony radius reached 700 μm. In the contact inhibition region, the average cell movement rate was always homogeneous and decreased to zero when cell migration was stopped (Fig. 6C,F). In the proliferating ring at the peripheral region of the colony, the average cell movement rate decreased but was still heterogeneous when cell migration was stopped (Fig. 6C,F) and became homogeneous when cell division was stopped (Fig. 6B,E). This result confirmed that cell division was a factor that led to the heterogeneity of cell movement rate in colonies.

Supplementary video related to this article can be found at https://doi.org/10.1016/j.jbiosc.2018.10.016.

We tracked cell movement at the central and peripheral regions of colonies to understand how cell division affects cell movement rate. Results in Fig. 7A showed that cells at the central region of colonies moved randomly and fluctuated around the center of the colony while cells at the peripheral region of the colony migrated toward the periphery of the colony. Movie S6 shows that cells at the central region of the colony were not pushed by the other cells because they stayed in the contact inhibition region where cells were in a quiescent state and did not divide. In contrast, cells at the peripheral region were surrounded by other proliferating cells and were affected by the division of these other cells. The movie shows the pushing outward of cells at the peripheral region by the division of inner cells. We also calculated the frequency of cell pushing every 24 h to reveal the effect of cell pushing on cell movement. At the central region of the colony, no cell pushing was found from 24 h to 144 h. The average cell movement rate at the central region of the colony was small and showed little change as time passed (Fig. 7B). On the contrary, cells at the peripheral region of the colony were pushed by the division of inner cells (Fig. 7C). Thus, the average cell movement rate at the peripheral region of the colony was higher than that at the central region of the colony. This result indicated a directly proportional relationship between the frequency of cell pushing and the cell movement rate in colonies of hiPSCs.

Supplementary video related to this article can be found at https://doi.org/10.1016/j.jbiosc.2018.10.016.

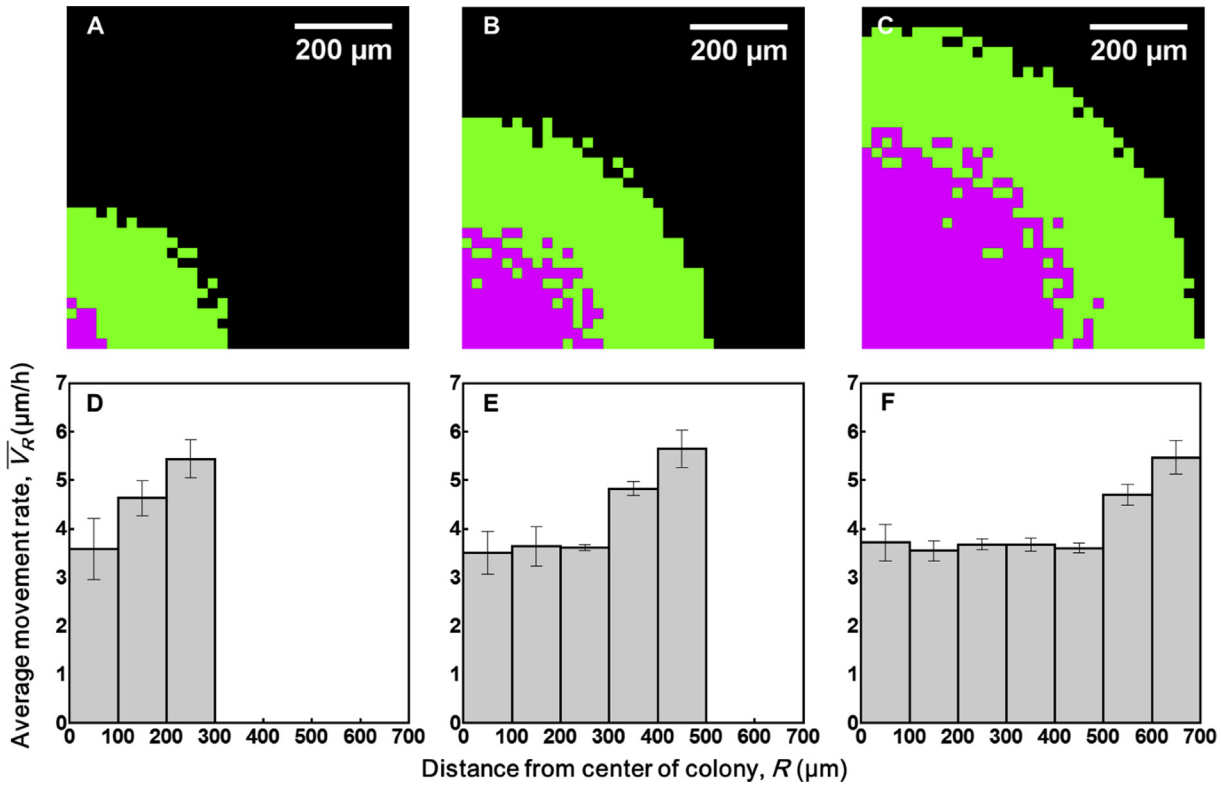

FIG. 5. *In silico* results at 50 h (A, D), 90 h (B, E), and 128 h (C, F): state of cells in a colony (A–C) (pink: quiescent state, green: proliferating state); average movement rate against the distance from the center of the colony (D–F).

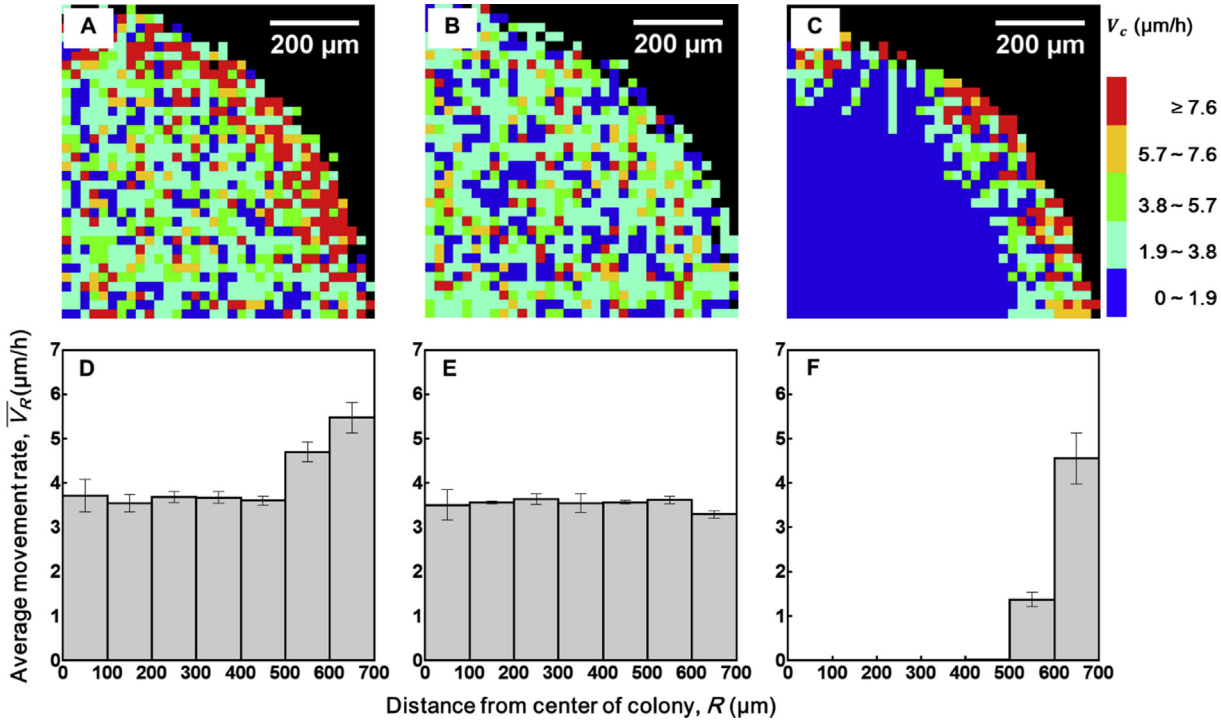

FIG. 6. *In silico* results when hiPSC colonies were cultured on MEF feeder cells under control conditions (A, D), when cell division was stopped (B, E), and when cell migration was stopped (C, F): heat map for movement rate of individual cells in one colony at 128 h (A–C); average movement rate against the distance from the center of the colony (D–F).

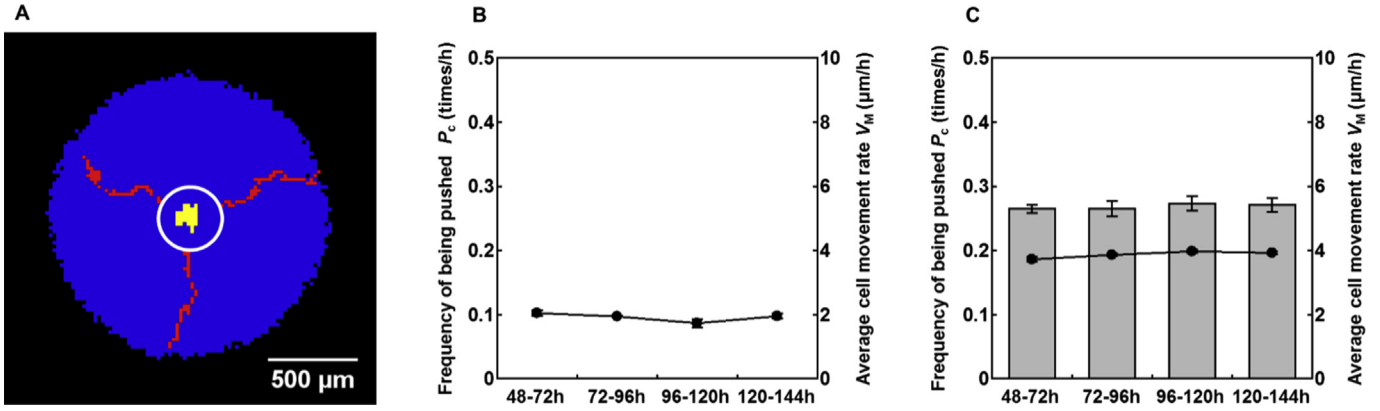

FIG. 7. *In silico* movement trajectory of three representative cells at the central region and at the peripheral region of the colony from $t = 24$ h to $t = 144$ h (A); *in silico* frequencies of cell pushing (columns) and cell movement rate (line) at the central region (B) and peripheral region (C) of the colony. Yellow cells: cells at the central region of colony at $t = 24$ h; red cells: cells at the peripheral region of colony at $t = 24$ h; blue cells: non-tracked cells at $t = 144$ h; white ring: edge of colony at $t = 24$ h.

DISCUSSION

We have presented new insights into the heterogeneity of average cell movement rate in colonies of hiPSCs using a stochastic discrete model. With a cell-based approach, the behaviors of every single cell were described by cell connection, cell migration, cell division, and cell quiescence rules. Even though rules of cell migration, cell division, and cell quiescence have been developed in our previous studies (11–13), this time we made some adjustments to study behaviors of human stem cells. Previously, cell migration rate was calculated from the migration rate of single isolated cells, which is difficult to estimate in hiPSC culture. Following the idea of controlling hiPSC fate through migration-dependent regulation of the balance between cell-cell and cell-substrate connections (15), we described cell connections in the context of energy for the first time. E_{max}, which is specific for each cell line, is used by cells to make connections and migrations. Connection energy and energy for migration can be compared to potential energy and kinetic energy in the physics field. We also extended rules for cell quiescence to describe the lesser degree of contact inhibition of stem cells compared with that of other cells. These improvements did not violate our previous rules but helped us overlap more target cells. In other words, this new model could likely be applied to our previous studies.

By fitting to experimental results, hiPSCs cultured on SNL feeder cells showed higher energy used for cell-cell connection than for cell-substrate connection which was the opposite effect observed in hiPSCs cultured on MEF feeder cells. We suggest that different feeder cells provided distinct topology surrounding hiPSCs that led to different cell-substrate connection energies and then indirectly affected cell-cell connection. This result is supported by the study by Moreno-Cencerrado et al. (16) where the strength of the cell-cell connection was shown to be highly influenced by the strength of the cell-substrate connection. The contact inhibition-related parameter N_c was also estimated by fitting to experimental data. When the number of cell layers for occurrence of contact inhibition N_c equaled 7 or 8, the result showed a lesser degree of contact inhibition in hiPSC cultures than in non-stem cell cultures as reported previously (11,13) where N_c equaled 1. After all parameters in this model were estimated and the appropriateness of the model was validated by comparing the simulated results with different experimental data sets. Since the results of simulations showed satisfactory agreement with data obtained from *in vitro* experiments, our developed model was considered to correctly describe hiPSC behaviors.

With the developed model, we executed simulations to understand the reason for the heterogeneity of average cell movement rate in colonies. We first found that the average movement rate was homogeneous in the contact inhibition region at the central region of the colony. However, in the proliferating region at the peripheral region of the colony, cell movement showed position-dependent characteristics that increased from the inside to the edge of colony. The difference in movement behavior between the contact inhibition region and the proliferating region implied the role of cell division in cell movement rates in a colony. After stopping cell migration or cell division and comparing to the control result, we found that both cell migration and cell division affected cell movement rates in a colony. However, cell division was the only factor that led to a higher cell movement rate at the peripheral region of the colony than at the central region of the colony. The cell pushing shown here came from the division rule where the mother cells push neighbor cells to make space for their daughter cells when there is no vacant space around the cell. This rule was also used in some papers for modeling cancer cells (17,18). In our study, there is a need to distinguish between the terms cell migration and cell movement. Cell migration is the ability of a cell to actively change to a new position. Meanwhile, cell movement is the overall change of cell position that may result from cell migration or by being pushed by the division of another cell. In the contact inhibition region, cell movement rate was only affected by cell migration. In contrast, at the peripheral region of the colony, cell movement rate was affected by both cell migration and cell pushing. Therefore, when the distance from the center of the colony increased, the frequency of cell pushing due to cell division increased, raising the average cell movement rate. This result confirmed our previous result about the effect of cell division on cell movement rate that cells at the peripheral region of the colony had a higher movement rate because they were pushed by inner cells.

With the full-discrete feature, our model has a disadvantage in simulating continuous processes such as cell migration. Instead of continuous changes in position, cell migration is described by the immediate change of cell position followed by waiting in the new position for a period of time. Additionally, a weakness of our CA model is that the uniform spacing makes it difficult to realize an increase in cell size during growth, mechanical constraint of cells in a population, or the multi-directionality of cell migration. However, any type of model has its pros and cons. The strength of our model is its lower computational cost than off-lattice models. Furthermore, since parameters are created based on phenomena,

parameter values can be estimated from *in vitro* observations or experimental data. More importantly, our model can realize the heterogeneity of cells in a colony that is impossible when using a continuous model. The model satisfied our final goal to develop a simple but efficient model for the hiPSCs engineering field. For future directions, we will develop a rule for deviating from the undifferentiated state of cells in a colony to understand more about this phenomenon. Understanding the mechanism of deviation phenomenon will provide much useful information in an effort to maintain hiPSCs in an undifferentiated state, which is crucial in cell processing.

Supplementary data to this article can be found online at https://doi.org/10.1016/j.jbiosc.2018.10.016.

ACKNOWLEDGMENTS

This research was supported by the Japan Agency for Medical Research and Development (AMED) under Grant Number JP15be0204428.

References

1. **Chowdhury, F., Li, Y., Poh, Y.-C., Yokohama-Tamaki, T., Wang, N., and Tanaka, T. S.:** Soft substrates promote homogeneous self-renewal of embryonic stem cells via downregulating cell-matrix tractions, PloS One, **5**, e15655 (2010).
2. **Serra, M., Brito, C., Correia, C., and Alves, P. M.:** Process engineering of human pluripotent stem cells for clinical application, Trends Biotechnol., **30**, 350–359 (2012).
3. **Chen, K. G., Mallon, B. S., McKay, R. D., and Robey, P. G.:** Human pluripotent stem cell culture: considerations for maintenance, expansion, and therapeutics, Cell Stem Cell, **14**, 13–26 (2014).
4. **Bratt-Leal, A. M., Carpenedo, R. L., and McDevitt, T. C.:** Engineering the embryoid body microenvironment to direct embryonic stem cell differentiation, Biotechnol. Prog., **25**, 43–51 (2009).
5. **Kim, M. H., Masuda, E., and Kino-oka, M.:** Kinetic analysis of deviation from the undifferentiated state in colonies of human induced pluripotent stem cells on feeder layers, Biotechnol. Bioeng., **111**, 1128–1138 (2014).
6. **Rosowski, K. A., Mertz, A. F., Norcross, S., Dufresne, E. R., and Horsley, V.:** Edges of human embryonic stem cell colonies display distinct mechanical properties and differentiation potential, Sci. Rep., **5**, 14218 (2015).
7. **Till, J. E., McCulloch, E. A., and Siminovitch, L.:** A stochastic model of stem cell proliferation, based on the growth of spleen colony-forming cells, Proc. Natl. Acad. Sci. USA, **51**, 29–36 (1963).
8. **Viswanathan, S. and Zandstra, P. W.:** Towards predictive models of stem cell fate, Cytotechnology, **41**, 75–92 (2003).
9. **MacArthur, B. D., Ma'ayan, A., and Lemischka, I. R.:** Systems biology of stem cell fate and cellular reprogramming, Nat. Rev. Mol. Cell Biol., **10**, 672–681 (2009).
10. **Herberg, M. and Roeder, I.:** Computational modelling of embryonic stem-cell fate control, Development, **142**, 2250–2260 (2015).
11. **Kino-oka, M., Umegaki, R., Taya, M., Tone, S., and Prenosil, J. E.:** Valuation of growth parameters in monolayer keratinocyte cultures based on a two-dimensional cell placement model, J. Biosci. Bioeng., **89**, 285–287 (2000).
12. **Kino-oka, M., Maeda, Y., Yamamoto, T., Sugawara, K., and Taya, M.:** A kinetic modeling of chondrocyte culture for manufacture of tissue-engineered cartilage, J. Biosci. Bioeng., **99**, 197–207 (2005).
13. **Kagawa, Y. and Kino-oka, M.:** An *in silico* prediction tool for the expansion culture of human skeletal muscle myoblasts, R. Soc. Open Sci., **3**, 160500 (2016).
14. **Shuzui, E., Kim, M. H., and Kino-oka, M.:** Anomalous cell migration triggers a switch to deviation from the undifferentiated state in colonies of human induced pluripotent stems on feeder layers, J. Biosci. Bioeng., **127**, 246–255 (2019).
15. **Kim, M. H. and Kino-oka, M.:** Maintenance of an undifferentiated state of human induced pluripotent stem cells through migration-dependent regulation of the balance between cell-cell and cell-substrate interactions, J. Biosci. Bioeng., **119**, 617–622 (2015).
16. **Moreno-Cencerrado, A., Iturri, J., Pecorari, I., Vivanco, M. D. M., Sbaizero, O., and Toca-Herrera, J. L.:** Investigating cell-substrate and cell-cell interactions by means of single-cell-probe force spectroscopy, Microsc. Res. Tech., **80**, 124–130 (2017).
17. **Stéphanou, A., Lesart, A. C., Deverchère, J., Juhem, A., Popov, A., and Estève, F.:** How tumour-induced vascular changes alter angiogenesis: insights from a computational model, J. Theor. Biol., **419**, 211–226 (2017).
18. **Forster, J. C., Douglass, M. J. J., Harriss-Phillips, W. M., and Bezak, E.:** Simulation of head and neck cancer oxygenation and doubling time in a 4D cellular model with angiogenesis, Sci. Rep., **7**, 11037 (2017).